

Prediction of the collisions of meteoroids originating in comet 21P/Giacobini-Zinner with the Mercury, Venus, and Mars

D. Tomko^a, L. Neslušan^a

^a*Astronomical Institute, Slovak Academy of Science, 05960 Tatranská Lomnica, Slovakia*

ARTICLE INFO

Keywords:

meteoroid-stream parent body
dynamics of meteoroid stream
comet 21P/Giacobini-Zinner
meteor showers on terrestrial planets

ABSTRACT

After the prediction of meteor showers in the Earth's atmosphere caused by the particles originating in the nucleus of comet 21P/Giacobini-Zinner, we went on with the prediction of showers on the other three terrestrial planets. Based on our modeling of theoretical stream of the parent comet, we predicted several related meteorite (on Mercury) or meteor (on Venus and Mars) showers. There occurred the filaments, in the stream, with the particles coming to each planet from a similar direction. We found that this is a consequence of the specific distribution of argument of perihelion (peaked close to the value of 180°) and longitude of ascending node of the stream, and that the particles collide with each planet in an arc of their orbits being close to perihelion.

1. Introduction

A number of meteoroid streams move in the interplanetary space. When a planet crosses the spatial corridor in which a stream moves, the meteoroid particles collide either with its atmosphere or surface. A meteor shower can then be detected. We know a lot of meteor showers that can be observed in the atmosphere of our planet, the Earth.

However, the collisions of meteoroids also happen with the other planets. At the present, there are no observational stations to detect the meteors (or meteorites) on the other planets. However, we can predict an existence of meteor showers if other planet passes, periodically, through a corridor of a stream, which is colliding with the Earth. Or, we can follow the dynamical evolution of stream originating in a particular cometary nucleus or asteroid, when we know or assume that the object is a source of meteoroid particles.

In the past, the meteoroid streams colliding with the other terrestrial planets were studied by several authors (Beech, 1998; Christou et al., 2007; McAuliffe and Christou, 2005; Neslušan, 2005; Withers et al., 2007; Espley et al., 2010; Christou et al., 2012; Dmitriev et al., 2013; Withers et al., 2013; Christou et al., 2015a,b; Fries et al., 2015, 2016; Kuznetsova et al., 2018). The comprehensive review of meteor showers, which could probably be detected on Venus and Mars, was given by Christou (2010). Recently, Christou et al. (2019) published the review chapter about the “extra-terrestrial” meteors.

In this work, we deal with the meteoroids originating in the periodic comet 21P/Giacobini-Zinner in course to predict their collisions with the terrestrial planets Mercury, Venus, and Mars. In our earlier work (Neslušan and Tomko, 2023, Paper I, hereafter), we already modeled the stream of this comet and predicted the associated meteor showers observable in the Earth's atmosphere.

2. Method and models created

The method how the models of 21P's meteoroid stream were created was described in Paper I. These models can be used to predict the meteor showers observable at any terrestrial planet; in the atmosphere of Venus and Mars as well as the showers of meteorites impacting the surface of Mercury.

We briefly remind the method of model creation. In the first step, the nominal orbit of the parent comet, 21P, was integrated in time backward for an arbitrarily selected period, t_{ev} . In more detail, the integration was terminated exactly in the time of the comet's perihelion passage that was nearest to time t_{ev} before the present. In the perihelion, we assumed an ejection of 10,000 test particles from the comet's nucleus. The particles were ejected randomly to all

*Corresponding author: L. Neslušan
ne@ta3.sk (L. Neslušan)
ORCID(s): 0000-0001-9758-1144 (L. Neslušan)

directions with the same ejection speed equal to one thousandth heliocentric speed of the comet in its perihelion. The aim of this stream modeling was filling in the orbital phase space of the assumed stream with the particles; we did not intend to reproduce a real ejection of meteoroids from the surface of their parent body. In a further step, we followed, via a numerical integration, the dynamical evolution of the created set of the test particles up to the present, i.e. for the period of t_{ev} . Hence, t_{ev} is referred to as an evolutionary time.

In the forward integration, we assumed the Poynting-Robertson (P-R) effect influencing the motion of the particles (Klačka, 2014). The strength of this effect is characterized with a dimensionless parameter β . This parameter and the evolutionary time are supposed to be the free parameters in our modeling. In accord with Paper I, the models for all combinations of the values $t_{ev} = 0.5, 1, 2,$ and 4 kyr and $\beta = 10^{-11}, 10^{-4}, 0.001, 0.003,$ and 0.005 were considered. The results yielded by these models are described in the following section. The numerical integration was performed by using the integrator Gauss-Radau (RA15) (Everhart, 1985) within the MERCURY software package (Chambers, 1999; Chambers and Murison, 2000).

3. Results

In all models, the meteoroid stream splits to several filaments, the particles of which can be detected as individual meteor or meteorite showers on given planet. The mean planet-centric parameters and mean orbital elements of these filaments are given in Tables 1–6. These parameters were determined by averaging the parameters of individual particles with the minimum-orbit intersection distance (MOID), in respect to given planet, smaller than 0.02 au at the end of the numerical integration (i.e. at the present time). In tables, we denote the northern filaments with abbreviation “NF” and southern filaments with “SF”. We assigned a number to each filament, which follows the NF or SF.

The radiants of particles in selected models of each filament are shown in Figs. 1–3. In more detail, we selected the model, in which the given filament corresponded to the shower of category (i) (see below) and was represented by the largest number of particles. If there is no shower of category (i), then we selected the model of category (ii) with the largest number of particles. In the figures, the filaments are mutually distinguished by various colors and symbols. Although we describe the radiants on the sky of a planet other than Earth, we still use the common equatorial or ecliptical coordinate frames; it would be difficult and, likely, useless to define other, local, coordinate systems.

As stated by Marsden and Sekanina (1971) and confirmed in our Paper I, comet 21P has been in an erratic, rapidly changing orbit. This has caused a fast change of orbits in its meteoroid stream. The orbits of particles are dispersed enough and the filaments have often not well defined orbital corridor. Due to this circumstance, it was, in some cases, hard to decide if an accumulation of radiants or orbits is or is not a shower.

Thus, we divided the showers into three categories: (i) well recognizable, (ii) dispersed but still recognizable, and (iii) extremely dispersed. The division was rather intuitive than exact; we usually classified a shower in the first category when the determination errors (σ s) of its argument of perihelion, ω , and longitude of ascending node, Ω , were lower than $\sim 10^\circ$. Sometimes, there was a grouping of radiants, but σ of ω or Ω , or both exceeded $\sim 40^\circ$. Such a shower, even if really existed, could scarcely be recognized in a database of meteors or meteorites. We classified such very dispersed group of particles as belonging to category (iii). Finally, these groupings were omitted in a further consideration; they are not listed in the tables. The lines with the mean parameters of the showers of category (ii) are given in the brackets in the tables.

3.1. 21P’s meteorite showers observable on Mercury

Mercury is a planet without an atmosphere that could act on the particles moving toward its surface. Therefore, all meteoroids in the collisional course with this planet impact its surface. One can suppose that the microscopic particles are incorporated to the surface material of the planet. The larger particles obviously survive as the meteorites.

Term “meteor” refers to a phenomena in a planetary atmosphere, i.e. in a gaseous environment. A stream of meteoroids leads to a corresponding meteor shower. In the case of Mercury, this term should not be used. We will rather speak about a meteoroid stream impacting the first Solar-System planet.

Also in the case of Mercury, the 21P’ stream splits into several filaments colliding with the planet. In particular, the modeling of meteoroid stream resulted in the prediction of five Mercury’s meteoroid filaments with radiants on the northern sky and five filaments with radiants on the southern sky. The mean parameters characterizing these filaments are listed in Tables 1 (mean planet-centric parameters) and 2 (mean orbital elements). The radiants of the particles used to predict the filaments in selected models are in Fig. 1.

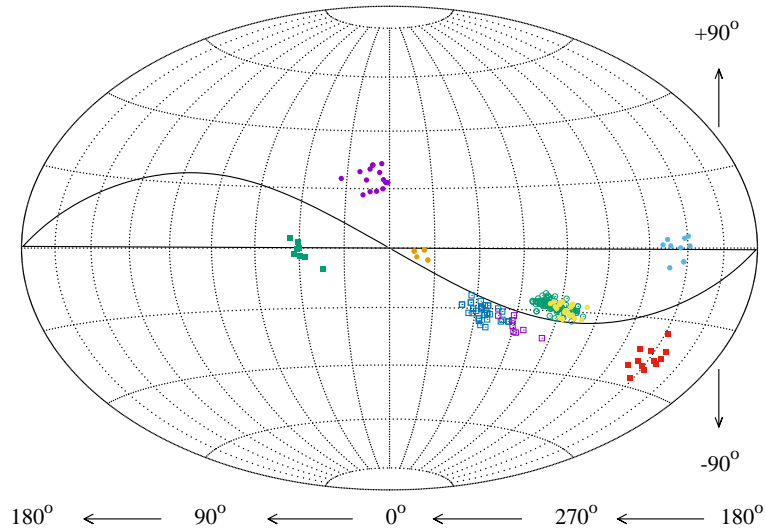


Figure 1: Positions of the radiants of theoretical particles in the atmosphere of Mercury associated with comet 21P. The positions are plotted in the Hammer projection of the celestial sphere. Equatorial coordinate frame is used. The sinusoid-like curve indicates the ecliptic. The radiants of the theoretical particles in the predicted filaments on the northern hemisphere NF1, NF3, NF4, and NF5 are shown with purple, turquoise, orange, and yellow full circles. Filament NF2 is shown with green empty circles. The radiants of the theoretical particles in the predicted filaments SF2 and SF3 on the southern hemisphere are shown with red and green full squares and filaments SF1 and SF4 with blue and purple empty squares. Full symbols are used for the radiants of showers of category (i) and empty symbols for category (ii).

The radiants of filaments NF1, NF3, and NF4 (purple, turquoise, and orange full circles, respectively) are well separated each other as seen in Fig. 1). The radiants of NF2 and NF5 (empty green and full yellow circles) are overwhelming. The particles of these two filaments however clearly differ each other by solar longitude (80.0° – 101.8° vs. 327.3° – 352.5°) and argument of perihelion (323.2° – 340.4° vs. 6.6° – 23.9°).

Also southern filaments SF1, and SF4 (blue and purple empty squares) have a common radiant area and can be distinguished by largely different solar longitude and argument of perihelion. Only SF2 and SF3 (red and green full squares) can be well distinguished among the other southern filaments.

3.2. 21P's meteor showers observable on Venus

Venus moves through the corridors of six northern and three southern filaments of stream of 21P (Fig. 2, Tables 3 and 4).

There is an interesting radiant area of filament NF2 (full turquoise circles in Fig. 2). It is narrow, but with a large extent in declination. This area is not separated from the radiant area of filament NF3 (full yellow circles), but filaments NF2 and NF3 can be well distinguished by their different mean angular distance from the Sun, γ , in time corresponding to the mean solar longitude. While $\gamma \geq 121^{\circ}$ in NF2, $\gamma < 86^{\circ}$ in NF3. The solar longitude, mean radiant, and mean angular orbital elements are also different.

Southern filament SF1 was predicted almost in every model that we constructed. However, the radiants of individual particles were, sometimes, so much dispersed that we could not regard it as a shower.

Filaments NF4, NF5, and NF6 were predicted in only two models. In NF4 and NF6, the parameters of the individual particles are relatively dispersed (showers of category (ii)). NF5 (red empty circles in Fig. 2) was predicted only with the help of a low number of particles. However, it is a quite compact, well-defined shower.

3.3. 21P's meteor showers observable on Mars

Our modeling of 21P' stream (described in Paper I) also predicted some showers, which could be observable in the atmosphere of Mars. Their mean planet-centric parameters are given in Table 5 and mean orbital elements in Table 6.

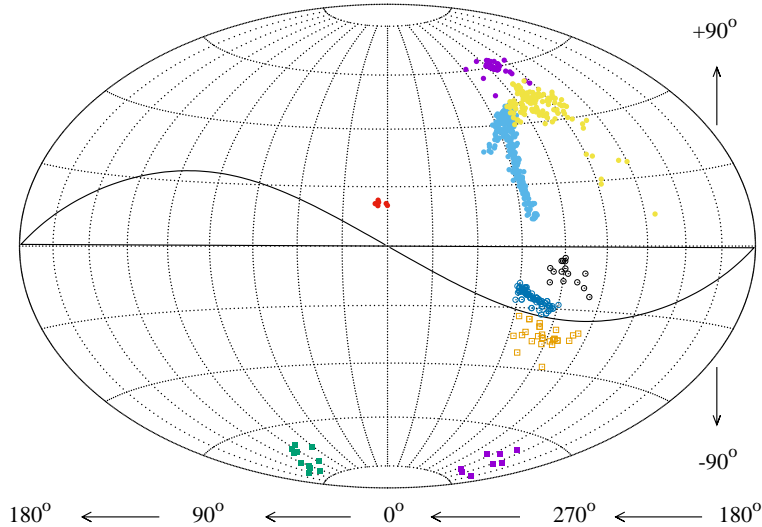


Figure 2: Positions of the radiant of theoretical particles in the atmosphere of Venus associated with comet 21P. The positions are plotted in the Hammer projection of the celestial sphere. Equatorial coordinate frame is used. The sinusoid-like curve indicates the ecliptic. The radiants of the theoretical particles in the predicted filaments on the northern hemisphere NF1, NF2, NF3, and NF5 are shown with purple, turquoise, yellow, and red full circles. Filaments NF4 and NF6 are shown with green and black empty circles. The radiants of the theoretical particles on the southern hemisphere in the predicted filament SF1 are shown with orange empty squares and those of filaments SF2 and SF3 with purple and blue full squares. Full symbols are used for the radiants of showers of category (i) and empty symbols for category (ii).

The positions of radiants of particles in the individual filaments, as predicted by the selected models, are shown in Fig. 3.

In total, the modeling predicted eleven northern and five southern showers, observable on this planet, which originated in 21P. Some of the predicted filaments (NF5, NF6, NF7, NF9, and NF11) are, however, questionable and should be considered with a caution. Filament NF8 (radiants shown with the black empty circles in Fig. 3) has also a largely dispersed radiants. We eventually consider it (shower category (ii)) since the values of its mean perihelion distance, eccentricity, argument of perihelion, longitude of ascending node, and geocentric velocity are predicted very similar in all five models that yielded this filament.

In Fig. 3, one can see a complex of 21P' showers predicted on Mars. The radiant areas of the northern and ecliptical southern showers are the parts of a continuous area. Actually, we initially identified a lower number of filaments when starting this work based on the radiant positions. In the next stage, we noticed that some particles, in the preliminary identified filaments, had different characteristics than a main group and can be distinguished as a separate group or more groups. We separated these groups as extra filaments.

Similarly to some showers predicted on Venus, also showers predicted on Mars have a narrow, but extended-in-declination radiant area. This property is remarkable in the case of the radiant area of NF1 (full purple circles in Fig. 3). A reason for the narrowness of this radiant area is unknown. The perihelion distance close to the orbit of Mars is not, probably, the reason, since there are other filaments with such a large perihelion distance, but their radiant area is not so narrow.

3.4. On the common direction of radiants

When we compare Figs. 2 and 3 with the radiants of 21P's meteors on Venus and Mars, and Fig. 3a,c,e in Paper I with the radiants of 21P's meteors on Earth, we can see that the particles come to each of these planets from similar directions.

If we analyze the orbital geometry of the particles in concerning filaments, we can find some interesting features. The mean perihelia of the filaments are situated at the orbit of given planet (cf. $q \sim 0.72$ au for the Venus' filaments, $q \sim 1.0$ au for the Earth's, and $q \sim 1.4$ au for the Mars' filaments). The particles can collide with a given planet only

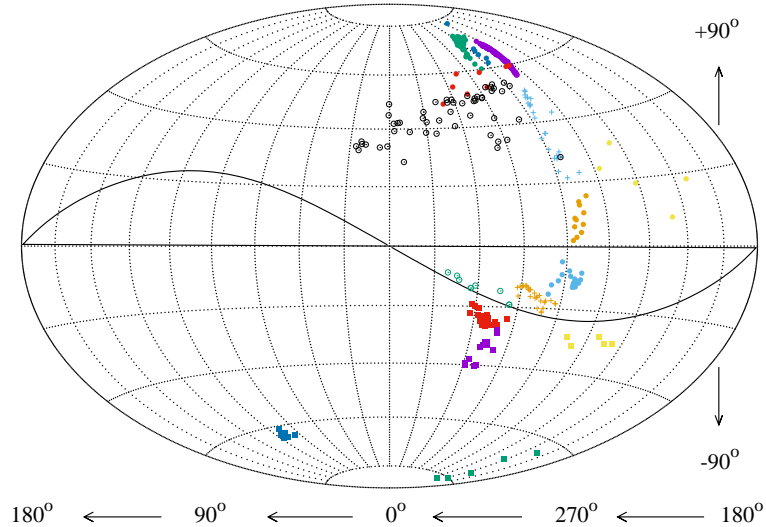


Figure 3: Positions of the radiants of theoretical particles in the atmosphere of Mars associated with comet 21P. The positions are plotted in the Hammer projection of the celestial sphere. Equatorial coordinate frame is used. The sinusoid-like curve indicates the ecliptic. The radiants of the theoretical particles in the predicted filaments on the northern hemisphere NF1, NF2, NF5, NF6, NF7, NF10, and NF11 are shown with purple, green, yellow, blue, red, turquoise, and orange full circles, respectively. Filaments NF3 and NF4 are shown with turquoise and orange crosses, and filaments NF8 and NF9 with black and green empty circles. The radiants of the theoretical particles in the predicted filaments on the southern hemisphere of sky SF1, SF2, SF3, SF4, and SF5 are shown with yellow, blue, red, purple, and green full squares. Full symbols and crosses are used for the radiants of showers of category (i) and empty symbols for category (ii).

in an arc of their orbits close to the perihelia because the argument of perihelion, ω , of a prevailing part of the whole stream is close to 180° (Fig. 4) or 0° (the second, smaller peak in the ω -distribution). Since the distribution of longitude of ascending node, Ω , of the whole stream is also compact, peaked at the values ranging from $\sim 180^\circ$ to $\sim 200^\circ$ (with a small, second peak at $\sim 10^\circ$ to $\sim 40^\circ$), the incoming direction of colliding particles is then almost unique.

In Fig. 4, we can see a high peak in the distribution of ω in several selected models with the abundant filaments. For $t_{ev} = 1$ kyr, the peak is narrow as for a weak ($\beta = 10^{-11}$ or $\beta = 10^{-4}$) as for a relatively strong ($\beta = 0.003$ or $\beta = 0.005$) P-R effect. It is also narrow in the model for $t_{ev} = 0.5$ kyr and $\beta = 10^{-11}$ and its width is not much larger either in the model for $t_{ev} = 2$ kyr and $\beta = 10^{-11}$. Despite the orbits of particles in the 21P' stream are rapidly changing, the argument of perihelion seems to be stable. The same can be observed for the longitude of ascending node of a prevailing part of particles in stream. On the other-hand side, the perihelia in the stream are predicted to be distributed throughout almost whole region of terrestrial planets, from ~ 0.3 to ~ 2.4 au.

4. Summary and conclusion

Using the resultant data of the modeling of meteoroid stream of comet 21P/Giacobini-Zinner, described in Paper I, we analyzed the close approaches of the particles, representing the meteoroids, to the orbits of Mercury, Venus, and Mars (the analysis concerning the Earth was done in the past and results published in Paper I).

We found several filaments of 21P' stream approaching the orbit of each of these three planets. On the basis of mean characteristics of these filaments, we predicted corresponding meteorite or meteor showers, which could be detected on each planet. Specifically, we found 5 (4), 6 (3), and 11 (5) northern (southern) showers on Mercury, Venus, and Mars, respectively. However, the radiants of particles of some predicted showers were rather dispersed onto a relatively large area of sky. The orbital elements were dispersed correspondingly. We classified these showers as the less certain showers of category (ii). Of the total number, 1 (2), 2 (1), and 2 (0) northern (southern) predicted showers were the showers of category (ii) at Mercury, Venus, and Mars, respectively.

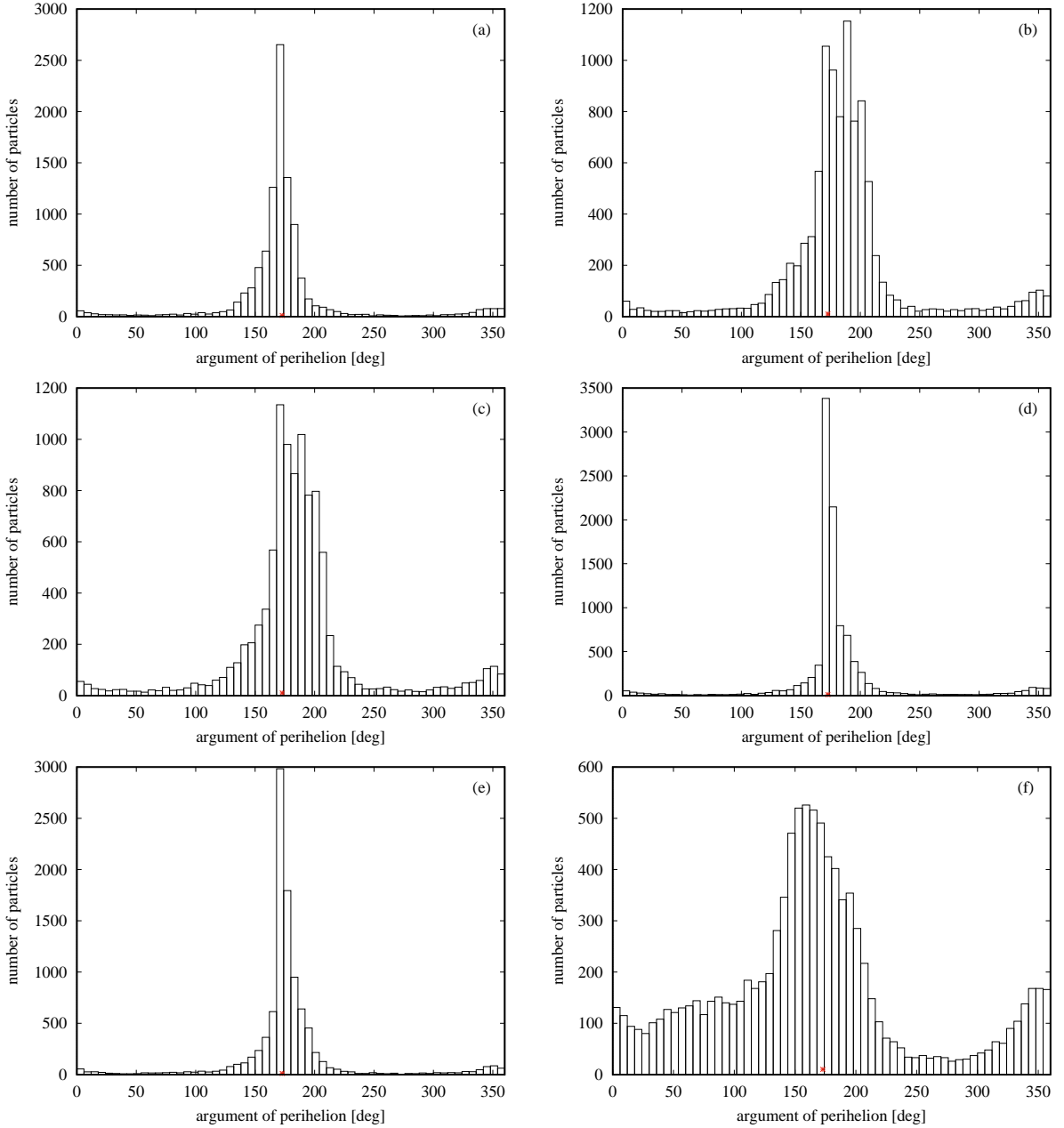


Figure 4: Distributions of the argument of perihelion, ω , in the models for $(t_{ev}, \beta) = (0.5 \text{ kyr}, 10^{-11})$ (panel a), $(1 \text{ kyr}, 10^{-11})$ (b), $(1 \text{ kyr}, 10^{-4})$ (c), $(1 \text{ kyr}, 0.003)$ (d), $(1 \text{ kyr}, 0.005)$ (e), and $(2 \text{ kyr}, 10^{-11})$ (f). An asterisk at the horizontal coordinate axis indicates the value of ω of the nominal orbit of parent comet.

Taking into account also the result given in Paper I, which dealt with the prediction of 21P' showers at the Earth, we found that, except of few minor showers, the positions of radiant areas of the showers predicted at Venus, Earth, and Mars are similar, i.e. the meteoroids hit each planet incoming from a similar direction. We explained this phenomenon by the orbital geometry of the 21P' stream: the distributions of argument of perihelion and longitude of ascending node have a dominant, high peak, which is conserved a relatively long time despite a rapid change of orbits. The value of argument of perihelion corresponding to the peak is close to 180° , therefore the particles hit each planet at their perihelia.

Our modeling also showed that a lot of particles predicted to hit a terrestrial planet have a chaotic radiant distributions, therefore they do not belong to any shower. Comet 21P significantly contributes to the sporadic meteorites or meteors which can be detected on any terrestrial planet.

Acknowledgements. This work was supported, in part, by the VEGA - the Slovak Grant Agency for Science, grant No. 2/0009/22, and by the Slovak Research and Development Agency under the contract No. APVV-19-0072.

References

- Beech, M., 1998. Venus-intercepting meteoroid streams. *MNRAS* 294, 259–264. doi:10.1046/j.1365-8711.1998.01178.x.
- Chambers, J.E., 1999. A hybrid symplectic integrator that permits close encounters between massive bodies. *Monthly Notices of the Royal Astronomical Society* 304, 793–799. doi:10.1046/j.1365-8711.1999.02379.x.
- Chambers, J.E., Murison, M.A., 2000. Pseudo-High-Order Symplectic Integrators. *Astronomical Journal* 119, 425–433. doi:10.1086/301161, arXiv:astro-ph/9910263.
- Christou, A., Killen, R.M., Burger, M.H., 2015a. A seasonal feature in Mercury's exosphere caused by meteoroids from comet Encke, in: AAS/Division for Planetary Sciences Meeting Abstracts #47, p. 107.02.
- Christou, A., Vaubaillon, J., Withers, P., Hueso, R., Killen, R., 2019. Extra-Terrestrial Meteors, in: Ryabova, G.O., Asher, D.J., Campbell-Brown, M.J. (Eds.), *Meteoroids: Sources of Meteors on Earth and Beyond*, p. 119.
- Christou, A.A., 2010. Annual meteor showers at Venus and Mars: lessons from the Earth. *MNRAS* 402, 2759–2770. doi:10.1111/j.1365-2966.2009.16097.x.
- Christou, A.A., Killen, R.M., Burger, M.H., 2015b. The meteoroid stream of comet Encke at Mercury: Implications for Mercury Surface, Space ENvironment, GEOchemistry, and Ranging observations of the exosphere. *Geophysical Research Letters* 42, 7311–7318. doi:10.1002/2015GL065361.
- Christou, A.A., Oberst, J., Elgner, S., Flohrer, J., Margonis, A., McAuliffe, J.P., Koschny, D., 2012. Orbital observations of meteors in the Martian atmosphere using the SPOSH camera. *Planetary and Space Science* 60, 229–235. doi:10.1016/j.pss.2011.09.002.
- Christou, A.A., Vaubaillon, J., Withers, P., 2007. The dust trail complex of comet 79P/du Toit-Hartley and meteor outbursts at Mars. *A&A* 471, 321–329. doi:10.1051/0004-6361:20077575.
- Dmitriev, V., Lupovka, V., Christou, A., Oberst, J., 2013. Meteoroid population near Mars, in: *European Planetary Science Congress*, pp. EPSC2013–629.
- Espley, J.R., Morgan, D.D., Christou, A., Farrell, W., Grebowsky, J., Gurnett, D., Plaut, J., 2010. MARSIS Observations of the 2009 Martian Geminid Meteor Shower: Null Results, in: *41st Annual Lunar and Planetary Science Conference*, p. 2187.
- Everhart, E., 1985. An efficient integrator that uses Gauss-Radau spacings, in: Carusi, A., Valsecchi, G.B. (Eds.), *IAU Colloq. 83: Dynamics of Comets: Their Origin and Evolution*, p. 185. doi:10.1007/978-94-009-5400-7_17.
- Fries, M., Christou, A., Archer, D., Conrad, P., Cooke, W., Eigenbrode, J., ten Kate, I.L., Matney, M., Niles, P., Sykes, M., Steele, A., Treiman, A., 2015. A Meteor Shower Origin for Martian Methane, in: LPI Editorial Board (Ed.), *78th Annual Meeting of the Meteoritical Society*, p. 5286.
- Fries, M., Christou, A., Archer, D., Conrad, P., Cooke, W., Eigenbrode, J., ten Kate, I.L., Matney, M., Niles, P., Sykes, M., Steele, A., Treiman, A., 2016. Martian Atmospheric Methane Plumes from Meteor Shower Infall: A Hypothesis, in: LPI Editorial Board (Ed.), *Sixth International Conference on Mars Polar Science and Exploration*, p. 6076.
- Klačka, J., 2014. Solar wind dominance over the Poynting-Robertson effect in secular orbital evolution of dust particles. *Monthly Notices of the Royal Astronomical Society* 443, 213–229. doi:10.1093/mnras/stu1133, arXiv:1401.0581.
- Kuznetsova, D., Gritsevich, M., Silber, E.A., Christou, A., 2018. Analytical Model for Determining the Outcome of Meteoroid Entry into the Martian Atmosphere, in: *81st Annual Meeting of the Meteoritical Society*, p. 6198.
- Marsden, B.G., Sekanina, Z., 1971. Comets and Nongravitational Forces. IV. *Astronomical Journal* 76, 1135. doi:10.1086/111232.
- McAuliffe, J.P., Christou, A.A., 2005. Simulating Meteor Shower Observations In The Martian Atmosphere, in: AAS/Division for Planetary Sciences Meeting Abstracts #37, p. 27.09.
- Neslušan, L., 2005. The potential meteoroid streams crossing the orbits of terrestrial planets. *Contributions of the Astronomical Observatory Skalnaté Pleso* 35, 163–179.
- Neslušan, L., Tomko, D., 2023. Long-period dynamical evolution of the meteoroid stream originating in comet 21P/Giacobini-Zinner. *Icarus* 392, 115375. doi:10.1016/j.icarus.2022.115375.
- Withers, P., Christou, A.A., Vaubaillon, J., 2013. Meteoric ion layers in the ionospheres of venus and mars: Early observations and consideration of the role of meteor showers. *Advances in Space Research* 52, 1207–1216. doi:10.1016/j.asr.2013.06.012.
- Withers, P., Mendillo, M., Paetzold, M., Tellmann, S., Christou, A., Vaubaillon, J., 2007. Comparison Of Ionospheric Observations And Dynamical Predictions Of Meteor Showers At Mars, in: AAS/Division for Planetary Sciences Meeting Abstracts #39, p. 59.08.

A. Tabular information

Table 1

The mean planet-centric parameters of the showers associated with the comet 21P/Giacobini-Zinner, which are predicted to be seen on Mercury. In the individual columns, the following mean parameters are given: t_{ev} – the evolutionary time; β – the parameter characterizing the strength of non-gravitational force in respect to the gravity of the Sun, λ_{\odot} – the mean solar longitude; λ_{\odot}^{min} and λ_{\odot}^{max} are the minimum and maximum solar longitudes of the shower; these values delimit the shower activity; α and δ are the mean equatorial coordinates of the planet-centric radiant; V_{pc} is the mean planet-centric velocity; γ is the angular distance of mean radiant from the Sun in time corresponding to λ_{\odot} ; and n is the number of particles in the predicted shower (the total number of the particles in each model was 10,000).

t_{ev} [kyr]	β [1]	λ_{\odot} [deg]	$\lambda_{min}-\lambda_{max}$ [deg]	α [deg]	δ [deg]	V_{pc} km s ⁻¹	γ [deg]	n
filament NF1								
0.5	10 ⁻¹¹	74.8 ± 3.1	71.2–79.2	7.0 ± 3.2	16.3 ± 1.5	22.8 ± 1.9	63.	6
0.5	10 ⁻⁴	85.6 ± 5.8	80.0–94.5	12.8 ± 6.9	21.4 ± 2.5	19.2 ± 3.4	66.	6
1	10 ⁻¹¹	93.4 ± 1.6	91.5–96.3	13.2 ± 8.3	26.1 ± 1.6	16.6 ± 3.7	72.	14
1	10 ⁻⁴	93.0 ± 3.1	87.9–97.3	11.4 ± 8.5	25.7 ± 1.9	16.1 ± 4.0	73.	10
1	0.001	93.4 ± 2.1	90.1–96.3	16.0 ± 5.2	26.1 ± 2.5	18.0 ± 3.7	70.	6
1	0.003	88.7 ± 6.9	79.3–96.5	10.2 ± 7.6	23.8 ± 3.7	18.9 ± 4.6	71.	12
1	0.005	87.2 ± 7.2	77.6–98.6	7.8 ± 5.7	23.5 ± 3.5	18.3 ± 3.5	72.	15
2	10 ⁻⁴	99.6 ± 9.2	88.2–109.1	24.1 ± 7.6	27.1 ± 4.2	20.0 ± 3.9	68.	7
2	0.001	96.7 ± 13.5	81.5–116.0	22.8 ± 10.8	25.1 ± 7.0	20.0 ± 3.9	67.	8
2	0.003	107.8 ± 1.7	104.3–109.7	26.2 ± 9.6	28.6 ± 2.9	17.0 ± 2.9	74.	8
2	0.005	104.6 ± 3.7	95.5–109.5	27.4 ± 7.8	28.7 ± 1.7	19.2 ± 3.4	70.	13
filament NF2								
[0.5	10 ⁻¹¹	81.2 ± 5.9	70.7–94.1	273.1 ± 6.2	-19.5 ± 1.4	31.1 ± 0.7	168.	56]
[0.5	10 ⁻⁴	81.0 ± 5.0	70.3–89.7	272.9 ± 4.9	-19.3 ± 1.5	31.1 ± 0.7	168.	33]
[0.5	0.001	80.0 ± 2.6	74.4–85.8	271.7 ± 2.9	-19.6 ± 1.1	31.1 ± 0.8	168.	27]
[1	10 ⁻¹¹	90.0 ± 6.3	73.6–101.4	283.3 ± 6.4	-18.4 ± 1.6	31.6 ± 0.7	167.	105]
[1	10 ⁻⁴	90.9 ± 4.0	79.4–99.0	284.3 ± 3.7	-18.3 ± 1.8	31.6 ± 0.6	167.	56]
[1	0.001	92.4 ± 4.4	76.7–102.8	288.5 ± 13.3	-15.9 ± 8.5	30.7 ± 4.5	163.	44]
[1	0.003	84.4 ± 8.0	69.2–98.8	279.5 ± 15.9	-17.0 ± 7.7	30.7 ± 4.3	164.	49]
[1	0.005	83.9 ± 9.6	57.3–100.1	277.8 ± 9.5	-19.0 ± 1.7	32.2 ± 1.4	166.	93]
[2	10 ⁻¹¹	101.8 ± 4.9	96.2–109.6	296.2 ± 4.5	-17.1 ± 1.7	31.8 ± 1.2	166.	15]
[2	10 ⁻⁴	93.6 ± 5.4	88.6–103.8	287.7 ± 5.4	-17.9 ± 1.3	31.9 ± 0.7	166.	14]
[2	0.001	93.6 ± 6.5	84.0–109.0	287.7 ± 6.0	-18.3 ± 2.2	31.8 ± 1.2	166.	16]
[2	0.003	100.9 ± 5.4	89.0–113.0	299.6 ± 3.5	-16.7 ± 1.6	33.7 ± 1.3	162.	37]
[2	0.005	94.2 ± 8.7	72.4–109.5	292.6 ± 7.0	-17.7 ± 1.6	33.6 ± 1.6	162.	40]
filament NF3								
1	0.001	321.6 ± 5.9	314.5–330.7	206.4 ± 5.2	3.0 ± 3.8	24.3 ± 2.7	118.	5
1	0.003	322.9 ± 15.1	303.8–336.3	208.3 ± 14.8	2.3 ± 5.5	23.4 ± 2.1	117.	6
1	0.005	314.9 ± 2.5	312.6–319.3	199.3 ± 3.2	3.5 ± 1.6	26.6 ± 1.6	118.	6
2	0.005	337.2 ± 4.8	330.1–344.6	225.0 ± 5.1	-0.2 ± 3.1	20.7 ± 3.0	114.	10
filament NF4								
2	10 ⁻¹¹	0.3 ± 2.0	-2.1–2.7	345.9 ± 2.7	-2.0 ± 1.6	31.5 ± 0.7	14.	7
filament NF5								
[1	10 ⁻⁴	330.1 ± 6.6	317.9–337.0	319.5 ± 6.8	-12.3 ± 1.6	30.8 ± 0.4	12.	7]
1	0.001	335.5 ± 9.2	321.7–344.0	323.4 ± 8.1	-10.7 ± 2.6	31.5 ± 0.7	14.	14
1	0.003	338.6 ± 6.7	324.5–351.0	325.4 ± 5.2	-10.2 ± 1.7	32.1 ± 1.3	15.	19
[1	0.005	327.3 ± 15.6	300.0–347.4	315.0 ± 14.2	-14.2 ± 3.6	32.0 ± 1.3	14.	12]
[2	10 ⁻¹¹	332.5 ± 6.0	322.2–338.4	320.7 ± 5.1	-12.6 ± 2.2	31.7 ± 0.5	14.	7]
[2	10 ⁻⁴	339.0 ± 4.2	330.8–342.6	326.5 ± 3.6	-9.0 ± 2.3	31.5 ± 0.3	14.	11]
[2	0.001	345.5 ± 10.2	330.3–359.8	318.8 ± 35.1	-6.9 ± 2.3	30.8 ± 3.8	28.	24]
[2	0.003	352.5 ± 7.9	338.6–366.8	336.8 ± 5.9	-5.9 ± 2.3	32.8 ± 1.3	17.	26]
[2	0.005	349.6 ± 9.7	328.6–364.3	332.5 ± 7.2	-7.8 ± 2.3	33.6 ± 1.9	18.	34]

Table 1
– continuation.

t_{ev} [kyr]	β [1]	λ_{\odot} [deg]	$\lambda_{min}-\lambda_{max}$ [deg]	α [deg]	δ [deg]	V_{pc} km s ⁻¹	γ [deg]	n
filament SF1								
[0.5	10 ⁻¹¹	309.3 ± 7.0	297.6–322.9	300.1 ± 7.2	-24.7 ± 2.3	31.1 ± 0.5	13.	21]
[0.5	10 ⁻⁴	306.5 ± 4.3	301.3–315.1	297.8 ± 3.9	-25.3 ± 1.3	30.8 ± 0.5	12.	15]
[0.5	0.001	312.0 ± 7.1	300.1–324.5	302.3 ± 6.9	-23.4 ± 2.0	31.4 ± 0.7	13.	18]
[0.5	0.003	302.5 ± 10.0	289.9–314.4	293.4 ± 10.8	-26.2 ± 1.6	30.8 ± 0.6	12.	8]
[1	10 ⁻¹¹	321.3 ± 6.4	307.8–329.3	312.9 ± 6.6	-22.5 ± 2.3	31.0 ± 0.5	13.	23]
[1	10 ⁻⁴	324.5 ± 6.1	310.8–335.4	315.9 ± 6.0	-21.2 ± 2.5	31.1 ± 0.5	13.	33]
[1	0.001	322.9 ± 6.8	307.7–334.1	313.9 ± 6.7	-21.8 ± 2.5	31.3 ± 0.4	13.	38]
[1	0.003	326.8 ± 6.7	312.9–336.2	318.4 ± 6.8	-20.8 ± 2.7	31.1 ± 0.2	13.	17]
[1	0.005	316.1 ± 10.1	294.9–333.2	307.5 ± 10.4	-23.8 ± 2.5	31.1 ± 0.5	13.	41]
[2	10 ⁻¹¹	330.8 ± 7.2	321.6–340.2	322.5 ± 7.3	-19.5 ± 2.5	30.9 ± 0.4	13.	9]
[2	10 ⁻⁴	331.2 ± 8.6	315.5–344.5	322.6 ± 8.2	-19.5 ± 2.7	31.1 ± 0.4	13.	12]
[2	0.003	315.2 ± 10.1	301.4–330.3	306.5 ± 10.2	-23.9 ± 3.3	30.9 ± 0.6	13.	13]
[2	0.005	330.4 ± 6.0	319.4–337.1	321.9 ± 5.7	-19.7 ± 2.6	30.9 ± 0.5	13.	11]
filament SF2								
1	10 ⁻¹¹	323.3 ± 3.5	319.1–328.4	201.6 ± 6.8	-26.3 ± 5.5	19.3 ± 5.2	112.	7
1	10 ⁻⁴	318.6 ± 6.8	310.5–328.2	197.9 ± 11.9	-25.4 ± 8.5	18.2 ± 4.0	111.	8
1	0.001	324.5 ± 5.4	316.8–333.0	202.7 ± 7.5	-27.0 ± 6.7	19.2 ± 4.1	112.	8
1	0.003	321.5 ± 6.8	314.2–332.8	197.6 ± 7.1	-22.9 ± 2.8	24.0 ± 3.7	116.	8
1	0.005	314.2 ± 3.7	308.7–321.1	192.8 ± 6.2	-24.0 ± 5.9	18.1 ± 5.0	112.	11
2	0.003	346.3 ± 13.8	327.9–358.0	224.3 ± 14.9	-30.4 ± 5.9	22.2 ± 4.3	115.	6
2	0.005	342.2 ± 5.4	335.2–351.0	220.2 ± 5.7	-31.5 ± 3.5	22.1 ± 4.0	114.	12
filament SF3								
2	0.005	103.0 ± 1.7	101.1–106.3	39.3 ± 4.5	-1.1 ± 3.2	20.2 ± 3.5	67.	8
filament SF4								
1	0.001	97.3 ± 5.5	90.3–105.2	291.1 ± 5.7	-25.3 ± 1.7	31.0 ± 0.4	168.	5
[1	0.003	91.8 ± 5.0	83.8– 98.7	286.1 ± 5.5	-26.1 ± 1.6	31.6 ± 0.7	167.	6]
[2	10 ⁻⁴	103.1 ± 7.1	88.3–112.8	298.6 ± 7.1	-25.5 ± 2.6	31.3 ± 0.5	167.	8]
[2	10 ⁻¹¹	83.7 ± 12.4	70.6–104.1	276.9 ± 14.2	-25.6 ± 1.9	31.6 ± 0.7	167.	6]
[2	0.003	97.0 ± 3.6	91.9–102.3	291.8 ± 3.8	-25.1 ± 1.7	31.4 ± 0.3	167.	7]
[2	0.005	105.5 ± 11.2	92.8–121.2	302.3 ± 11.4	-23.3 ± 2.4	31.7 ± 0.6	166.	7]

Table 2

The mean orbital elements of the showers associated with the comet 21P, which are predicted to be detected on Mercury. Quantities t_{ev} and β are the same as in Table 1.

t_{ev} [kyr]	β [1]	q [au]	e	ω [deg]	Ω [deg]	i [deg]
filament NF1						
0.5	10^{-11}	0.352 ± 0.014	0.881 ± 0.004	355.6 ± 1.6	13.5 ± 5.1	18.7 ± 1.7
0.5	10^{-4}	0.332 ± 0.016	0.886 ± 0.004	352.7 ± 3.5	30.1 ± 6.9	19.1 ± 2.3
1	10^{-11}	0.329 ± 0.013	0.886 ± 0.004	349.8 ± 3.7	41.7 ± 5.6	20.6 ± 2.3
1	10^{-4}	0.328 ± 0.013	0.887 ± 0.004	349.3 ± 4.3	41.9 ± 6.8	20.1 ± 2.0
1	0.001	0.327 ± 0.007	0.887 ± 0.002	351.4 ± 3.9	40.4 ± 6.0	21.3 ± 2.0
1	0.003	0.327 ± 0.014	0.887 ± 0.005	352.3 ± 4.7	34.9 ± 11.1	22.6 ± 5.1
1	0.005	0.319 ± 0.015	0.891 ± 0.005	352.0 ± 3.4	34.9 ± 11.1	23.3 ± 4.4
2	10^{-4}	0.319 ± 0.019	0.888 ± 0.005	353.8 ± 3.8	45.3 ± 12.8	22.3 ± 4.8
2	0.001	0.323 ± 0.015	0.887 ± 0.005	353.8 ± 3.4	41.5 ± 17.7	19.9 ± 4.9
2	0.003	0.293 ± 0.018	0.891 ± 0.005	351.5 ± 3.0	59.0 ± 4.2	19.9 ± 2.3
2	0.005	0.305 ± 0.011	0.886 ± 0.004	353.5 ± 3.4	52.7 ± 4.7	21.9 ± 3.4
filament NF2						
[0.5	10^{-11}	0.330 ± 0.024	0.889 ± 0.007	334.1 ± 19.7	43.2 ± 21.0	7.4 ± 3.4
[0.5	10^{-4}	0.331 ± 0.022	0.889 ± 0.006	332.9 ± 21.7	44.2 ± 22.9	7.9 ± 3.5
[0.5	0.001	0.333 ± 0.028	0.888 ± 0.008	339.6 ± 18.7	36.3 ± 18.7	8.0 ± 3.0
[1	10^{-11}	0.313 ± 0.023	0.893 ± 0.007	324.3 ± 21.0	63.8 ± 24.0	7.4 ± 2.9
[1	10^{-4}	0.314 ± 0.021	0.893 ± 0.006	324.5 ± 21.5	64.5 ± 21.7	7.8 ± 3.5
[1	0.001	0.313 ± 0.027	0.893 ± 0.008	329.8 ± 21.6	61.0 ± 23.1	9.3 ± 3.7
[1	0.003	0.316 ± 0.037	0.893 ± 0.010	331.1 ± 19.9	51.2 ± 23.9	8.9 ± 4.3
[1	0.005	0.296 ± 0.044	0.900 ± 0.013	330.2 ± 20.5	53.8 ± 24.5	7.4 ± 2.8
[2	10^{-11}	0.302 ± 0.038	0.896 ± 0.011	335.0 ± 23.3	66.3 ± 24.2	8.0 ± 2.8
[2	10^{-4}	0.304 ± 0.024	0.896 ± 0.007	323.2 ± 17.1	69.7 ± 21.5	7.5 ± 2.8
[2	0.001	0.304 ± 0.040	0.895 ± 0.012	326.4 ± 20.3	66.6 ± 23.1	7.3 ± 4.0
[2	0.003	0.230 ± 0.040	0.912 ± 0.012	340.4 ± 13.6	69.5 ± 13.2	8.1 ± 2.6
[2	0.005	0.233 ± 0.055	0.910 ± 0.014	334.8 ± 17.0	68.1 ± 17.7	8.0 ± 2.3
filament NF3						
1	0.001	0.348 ± 0.011	0.881 ± 0.003	4.2 ± 2.9	23.9 ± 6.2	20.8 ± 3.0
1	0.003	0.334 ± 0.016	0.885 ± 0.004	4.4 ± 2.0	23.0 ± 13.2	20.4 ± 2.5
1	0.005	0.346 ± 0.016	0.885 ± 0.004	1.9 ± 1.9	19.9 ± 1.9	19.5 ± 1.9
2	0.005	0.320 ± 0.012	0.883 ± 0.005	6.5 ± 3.0	32.3 ± 5.3	22.7 ± 4.0
filament NF4						
2	10^{-11}	0.297 ± 0.019	0.893 ± 0.006	11.0 ± 7.6	49.7 ± 10.8	8.3 ± 3.0
filament NF5						
[1	10^{-4}	0.329 ± 0.013	0.888 ± 0.004	7.8 ± 11.5	27.3 ± 13.8	8.4 ± 6.2
1	0.001	0.308 ± 0.023	0.894 ± 0.006	6.6 ± 5.9	31.3 ± 7.6	8.7 ± 2.8
1	0.003	0.289 ± 0.041	0.899 ± 0.012	11.5 ± 8.4	27.0 ± 9.3	7.8 ± 4.0
[1	0.005	0.293 ± 0.042	0.900 ± 0.012	23.9 ± 35.8	4.2 ± 34.0	5.7 ± 4.0
[2	10^{-11}	0.302 ± 0.016	0.897 ± 0.005	13.9 ± 13.3	20.5 ± 16.5	5.9 ± 3.3
[2	10^{-4}	0.308 ± 0.010	0.894 ± 0.003	12.1 ± 11.4	29.1 ± 14.3	9.5 ± 4.6
[2	0.001	0.292 ± 0.042	0.897 ± 0.012	11.3 ± 10.8	34.1 ± 10.7	10.8 ± 4.4
[2	0.003	0.258 ± 0.041	0.905 ± 0.012	14.1 ± 13.6	34.0 ± 16.0	7.7 ± 2.5
[2	0.005	0.232 ± 0.064	0.910 ± 0.019	20.3 ± 17.8	21.1 ± 18.9	6.8 ± 2.2

Table 2
– continuation.

t_{ev} [kyr]	β [1]	q [au]	e	ω [deg]	Ω [deg]	i [deg]
filament SF1						
[0.5	10^{-11}	0.332 ± 0.017	0.888 ± 0.005	205.5 ± 24.3	169.1 ± 23.1	$8.3 \pm 4.5]$
[0.5	10^{-4}	0.342 ± 0.018	0.885 ± 0.005	206.0 ± 24.1	167.2 ± 24.1	$8.6 \pm 3.7]$
[0.5	0.001	0.320 ± 0.024	0.891 ± 0.007	210.9 ± 27.1	165.3 ± 26.6	$6.3 \pm 2.9]$
[0.5	0.003	0.343 ± 0.023	0.886 ± 0.006	210.3 ± 15.7	159.0 ± 16.6	$8.1 \pm 3.3]$
[1	10^{-11}	0.334 ± 0.018	0.887 ± 0.006	212.7 ± 23.6	174.0 ± 23.2	$8.4 \pm 4.2]$
[1	10^{-4}	0.328 ± 0.017	0.889 ± 0.005	220.8 ± 29.2	168.5 ± 29.0	$7.5 \pm 4.2]$
[1	0.001	0.323 ± 0.013	0.890 ± 0.004	214.2 ± 25.4	172.9 ± 23.9	$8.0 \pm 4.4]$
[1	0.003	0.329 ± 0.012	0.889 ± 0.003	213.3 ± 17.6	178.6 ± 16.5	$7.4 \pm 3.2]$
[1	0.005	0.334 ± 0.018	0.890 ± 0.005	211.7 ± 23.6	169.9 ± 25.0	$8.8 \pm 4.3]$
[2	10^{-11}	0.332 ± 0.012	0.888 ± 0.003	217.1 ± 20.9	179.0 ± 19.8	$7.6 \pm 3.5]$
[2	10^{-4}	0.325 ± 0.014	0.890 ± 0.004	216.4 ± 31.5	179.1 ± 29.3	$8.7 \pm 4.1]$
[2	0.003	0.334 ± 0.021	0.886 ± 0.006	203.2 ± 26.5	177.5 ± 25.7	$10.5 \pm 5.1]$
[2	0.005	0.328 ± 0.014	0.887 ± 0.005	218.8 ± 27.1	176.3 ± 26.0	$7.8 \pm 3.0]$
filament SF2						
1	10^{-11}	0.332 ± 0.015	0.886 ± 0.005	188.5 ± 5.2	198.8 ± 5.0	20.3 ± 3.9
1	10^{-4}	0.332 ± 0.010	0.886 ± 0.003	189.7 ± 4.4	192.9 ± 3.8	19.6 ± 2.8
1	0.001	0.329 ± 0.014	0.886 ± 0.005	188.6 ± 4.3	199.5 ± 4.0	20.3 ± 2.1
1	0.003	0.336 ± 0.013	0.885 ± 0.004	184.0 ± 3.7	202.1 ± 8.2	23.1 ± 4.3
1	0.005	0.338 ± 0.012	0.886 ± 0.004	190.1 ± 5.2	189.1 ± 2.9	19.6 ± 2.6
2	0.003	0.320 ± 0.008	0.884 ± 0.004	185.0 ± 4.4	223.5 ± 13.0	19.8 ± 3.5
2	0.005	0.315 ± 0.012	0.881 ± 0.004	185.0 ± 4.2	218.0 ± 7.0	22.9 ± 5.0
filament SF3						
2	0.005	0.315 ± 0.013	0.883 ± 0.004	174.2 ± 3.6	229.0 ± 2.6	21.9 ± 2.4
filament SF4						
1	0.001	0.327 ± 0.009	0.889 ± 0.004	173.2 ± 5.6	220.6 ± 8.4	$8.4 \pm 3.1]$
[1	0.003	0.310 ± 0.022	0.894 ± 0.008	163.3 ± 18.6	226.9 ± 21.7	$8.1 \pm 4.3]$
[2	10^{-11}	0.311 ± 0.024	0.894 ± 0.007	158.5 ± 22.6	223.5 ± 31.1	$6.7 \pm 4.9]$
[2	10^{-4}	0.318 ± 0.011	0.891 ± 0.003	164.9 ± 10.8	236.2 ± 13.8	$9.9 \pm 4.3]$
[2	0.003	0.312 ± 0.009	0.892 ± 0.002	143.9 ± 22.2	251.3 ± 23.3	$5.5 \pm 3.2]$
[2	0.005	0.291 ± 0.015	0.892 ± 0.007	141.3 ± 31.1	265.3 ± 28.8	$6.5 \pm 3.1]$

Table 3

The mean planet-centric parameters of the showers associated with the comet 21P/Giacobini-Zinner, which are predicted to be seen on Venus. The same denotation as in Table 1 is used.

t_{ev} [kyr]	β [1]	λ_{\odot} [deg]	$\lambda_{min}-\lambda_{max}$ [deg]	α [deg]	δ [deg]	V_{pc} km s ⁻¹	γ [deg]	n
filament NF1								
0.5	10 ⁻¹¹	193.7 ± 2.6	182.8–199.4	275.7 ± 5.6	59.8 ± 2.0	22.7 ± 0.7	91.	67
0.5	10 ⁻⁴	194.0 ± 2.8	183.1–201.0	274.6 ± 5.1	59.7 ± 2.1	22.8 ± 0.8	91.	66
0.5	0.001	193.5 ± 1.3	187.2–197.2	277.0 ± 2.4	59.8 ± 1.3	22.7 ± 0.4	92.	52
1	10 ⁻⁴	198.6 ± 3.0	193.1–204.1	276.6 ± 7.3	63.0 ± 2.2	24.1 ± 1.0	92.	35
1	0.001	197.7 ± 4.1	191.0–205.4	277.9 ± 9.9	61.7 ± 2.7	23.8 ± 1.0	92.	32
1	0.003	197.0 ± 4.1	193.2–210.9	280.1 ± 11.0	62.2 ± 2.3	23.9 ± 0.8	93.	17
1	0.005	202.5 ± 5.3	192.2–211.5	270.9 ± 11.2	64.9 ± 2.8	25.7 ± 1.1	90.	10
2	10 ⁻¹¹	204.6 ± 8.5	189.1–222.3	288.5 ± 17.4	60.8 ± 4.1	23.4 ± 1.4	96.	16
2	10 ⁻⁴	205.7 ± 10.2	194.3–230.4	290.3 ± 18.0	61.6 ± 3.5	23.4 ± 0.8	97.	17
2	0.001	209.6 ± 11.7	193.5–228.3	287.8 ± 19.6	62.7 ± 5.8	24.4 ± 1.4	96.	11
2	0.003	205.5 ± 11.8	189.2–230.7	289.5 ± 20.6	62.0 ± 4.4	24.3 ± 0.9	97.	16
2	0.005	207.3 ± 9.3	192.3–222.2	278.6 ± 16.6	62.3 ± 4.8	24.4 ± 1.1	92.	12
filament NF2								
0.5	10 ⁻¹¹	142.1 ± 11.7	126.8–168.1	294.4 ± 4.3	19.1 ± 9.3	18.5 ± 0.8	136.	28
0.5	10 ⁻⁴	146.3 ± 13.5	130.8–175.2	294.5 ± 1.8	21.7 ± 9.9	18.2 ± 0.8	132.	18
0.5	0.001	157.6 ± 15.3	131.3–186.9	294.5 ± 7.6	29.3 ± 10.1	18.0 ± 0.9	123.	127
0.5	0.003	161.1 ± 14.8	130.9–189.4	296.2 ± 7.0	32.4 ± 10.6	18.3 ± 0.9	121.	243
1	10 ⁻⁴	156.1 ± 12.9	128.9–178.3	297.5 ± 2.6	29.3 ± 9.2	18.2 ± 0.9	125.	50
1	0.001	159.1 ± 14.5	132.3–192.0	300.3 ± 3.6	29.0 ± 11.9	18.6 ± 0.9	126.	123
1	0.003	162.6 ± 15.3	135.0–193.2	300.8 ± 3.7	30.5 ± 10.6	18.4 ± 0.8	124.	112
1	0.005	161.4 ± 14.7	134.3–186.1	300.1 ± 3.8	30.1 ± 10.7	18.4 ± 0.9	124.	135
2	10 ⁻¹¹	156.9 ± 17.5	139.8–190.2	304.0 ± 2.4	23.9 ± 11.9	18.8 ± 1.1	133.	8
filament NF3								
0.5	10 ⁻¹¹	200.1 ± 3.9	188.5–206.8	252.5 ± 8.2	39.1 ± 4.3	18.8 ± 1.1	69.	56
0.5	10 ⁻⁴	201.8 ± 7.2	182.8–224.2	250.0 ± 9.1	36.4 ± 6.6	19.2 ± 1.8	65.	54
0.5	0.001	199.5 ± 9.4	181.0–237.3	254.4 ± 28.4	39.5 ± 9.0	18.6 ± 1.5	70.	96
0.5	0.003	193.5 ± 7.5	181.2–221.4	266.2 ± 11.8	43.4 ± 5.8	18.0 ± 1.2	82.	110
0.5	0.005	193.8 ± 1.9	188.6–197.8	269.4 ± 3.9	49.8 ± 3.3	18.6 ± 1.0	86.	69
1	10 ⁻⁴	204.5 ± 16.5	183.0–234.0	264.3 ± 30.6	32.0 ± 12.8	19.6 ± 3.1	72.	17
1	0.001	198.4 ± 12.1	184.5–232.7	264.7 ± 15.2	40.8 ± 9.3	18.8 ± 2.5	78.	29
1	0.003	197.9 ± 9.5	184.8–231.0	269.3 ± 12.5	44.0 ± 6.7	18.5 ± 1.6	83.	57
1	0.005	198.4 ± 7.9	182.6–231.1	269.5 ± 10.4	45.2 ± 6.4	18.4 ± 1.6	83.	146
filament NF4								
[0.5	10 ⁻⁴	85.4 ± 7.1	72.6–100.0	275.0 ± 5.9	-20.4 ± 1.3	29.8 ± 1.3	170.	30]
[1	10 ⁻⁴	103.2 ± 8.5	86.1–117.3	292.5 ± 5.7	-16.7 ± 2.3	29.1 ± 1.8	170.	94]
filament NF5								
0.5	0.003	190.8 ± 1.5	188.7–192.0	3.1 ± 2.3	14.3 ± 0.7	23.5 ± 0.4	168.	6
0.5	0.005	192.0 ± 0.8	190.9–192.9	3.4 ± 0.8	15.5 ± 0.7	23.3 ± 0.2	167.	5
filament NF6								
[0.5	10 ⁻¹¹	157.8 ± 56.6	118.0–254.6	278.4 ± 6.3	-8.5 ± 3.5	16.6 ± 1.8	120.	15]
[0.5	0.003	122.4 ± 8.5	104.0–132.4	284.9 ± 5.1	-9.7 ± 5.0	18.3 ± 2.5	158.	15]

Table 3

– continuation.

t_{ev} [kyr]	β [1]	λ_{\odot} [deg]	$\lambda_{min}-\lambda_{max}$ [deg]	α [deg]	δ [deg]	V_{pc} km s ⁻¹	γ [deg]	n
filament SF1								
[0.5	10 ⁻⁴	257.5 ± 6.9	247.5–273.2	270.5 ± 6.5	-29.9 ± 3.1	19.5 ± 1.0	14.	13]
[0.5	0.005	267.1 ± 5.8	260.8–274.9	274.3 ± 1.3	-28.9 ± 1.6	22.1 ± 2.2	9.	8]
[1	10 ⁻¹¹	274.7 ± 28.9	143.6–304.2	291.4 ± 13.4	-29.1 ± 3.3	21.4 ± 2.2	16.	26]
[1	0.001	266.3 ± 32.5	132.6–287.4	283.2 ± 8.7	-28.4 ± 2.4	21.7 ± 1.7	16.	20]
[1	0.003	256.9 ± 50.3	109.4–290.6	282.1 ± 9.0	-28.8 ± 3.3	22.2 ± 1.4	24.	28]
[2	10 ⁻¹¹	260.3 ± 46.1	110.1–298.5	283.2 ± 11.2	-30.4 ± 5.7	21.6 ± 2.1	22.	25]
[2	10 ⁻⁴	271.6 ± 34.7	139.2–297.9	290.9 ± 10.6	-31.3 ± 5.2	21.5 ± 1.8	19.	18]
filament SF2								
1	0.003	229.8 ± 8.2	213.0–240.6	218.2 ± 24.1	-72.5 ± 4.5	20.3 ± 0.9	55.	9
[2	10 ⁻¹¹	236.7 ± 39.2	141.7–269.2	271.5 ± 27.1	-59.1 ± 6.6	19.8 ± 1.3	48.	14]
[2	10 ⁻⁴	240.1 ± 26.8	162.4–262.4	260.7 ± 33.0	-59.2 ± 7.0	20.6 ± 2.1	42.	12]
2	0.003	239.3 ± 5.3	231.0–245.0	242.8 ± 10.1	-64.1 ± 7.2	20.0 ± 0.7	44.	5
filament SF3								
1	0.001	226.4 ± 3.3	223.1–231.3	114.6 ± 12.0	-74.5 ± 3.9	25.1 ± 1.0	79.	5
2	10 ⁻¹¹	210.9 ± 12.3	193.0–232.7	90.2 ± 36.8	-69.5 ± 5.2	24.0 ± 3.0	88.	11
2	10 ⁻⁴	188.3 ± 7.0	175.6–196.1	106.2 ± 24.4	-72.8 ± 4.0	22.8 ± 1.8	84.	6
2	0.003	219.2 ± 5.2	211.7–225.3	105.5 ± 13.5	-70.3 ± 3.2	25.7 ± 0.9	83.	10
2	0.005	221.1 ± 5.9	213.5–230.1	111.4 ± 17.3	-72.5 ± 3.5	25.3 ± 1.0	81.	11

Table 4

The mean orbital elements of the showers associated with the comet 21P, which are predicted to be detected on Venus. Quantities t_{ev} and β are the same as in Table 1.

t_{ev} [kyr]	β [1]	q [au]	e	ω [deg]	Ω [deg]	i [deg]
filament NF1						
0.5	10^{-11}	0.726 ± 0.010	0.772 ± 0.003	183.3 ± 2.2	193.7 ± 1.9	34.7 ± 1.4
0.5	10^{-4}	0.723 ± 0.012	0.773 ± 0.004	182.9 ± 2.0	193.8 ± 2.1	34.8 ± 1.6
0.5	0.001	0.723 ± 0.012	0.773 ± 0.004	183.8 ± 1.0	193.7 ± 1.1	34.6 ± 0.9
1	10^{-11}	0.725 ± 0.012	0.777 ± 0.009	186.4 ± 5.7	192.4 ± 7.5	31.0 ± 6.2
1	10^{-4}	0.725 ± 0.012	0.768 ± 0.005	183.8 ± 2.8	198.8 ± 2.3	37.3 ± 2.0
1	0.001	0.721 ± 0.012	0.771 ± 0.005	184.0 ± 3.9	198.0 ± 2.7	36.5 ± 2.1
1	0.003	0.728 ± 0.010	0.772 ± 0.005	185.0 ± 4.5	197.7 ± 3.2	36.7 ± 1.5
1	0.005	0.716 ± 0.010	0.774 ± 0.005	182.1 ± 4.8	202.0 ± 4.7	40.2 ± 2.1
2	10^{-11}	0.723 ± 0.014	0.772 ± 0.005	186.8 ± 6.8	206.3 ± 6.5	35.2 ± 2.8
2	10^{-4}	0.722 ± 0.013	0.772 ± 0.004	187.6 ± 7.7	207.7 ± 8.1	35.4 ± 1.6
2	0.001	0.716 ± 0.014	0.770 ± 0.007	187.0 ± 8.5	211.3 ± 7.9	37.2 ± 3.3
2	0.003	0.719 ± 0.010	0.770 ± 0.005	187.6 ± 9.0	207.2 ± 8.7	36.9 ± 2.2
2	0.005	0.727 ± 0.011	0.767 ± 0.005	183.6 ± 7.0	207.3 ± 7.7	37.4 ± 2.6
filament NF2						
0.5	10^{-11}	0.727 ± 0.011	0.789 ± 0.003	189.0 ± 3.9	177.2 ± 4.8	18.8 ± 2.3
0.5	10^{-4}	0.732 ± 0.011	0.788 ± 0.003	189.4 ± 4.0	177.8 ± 4.6	19.1 ± 2.2
0.5	0.001	0.729 ± 0.012	0.789 ± 0.003	187.9 ± 3.3	180.5 ± 3.4	20.9 ± 2.1
0.5	0.003	0.729 ± 0.011	0.789 ± 0.004	188.8 ± 3.8	180.4 ± 3.8	21.9 ± 2.6
0.5	0.005	0.727 ± 0.011	0.788 ± 0.004	186.8 ± 3.1	184.6 ± 4.2	24.5 ± 2.7
1	10^{-4}	0.727 ± 0.012	0.789 ± 0.003	190.7 ± 4.6	180.1 ± 5.2	21.1 ± 2.3
1	0.001	0.724 ± 0.012	0.791 ± 0.004	190.6 ± 3.9	184.5 ± 4.9	21.1 ± 3.2
1	0.003	0.724 ± 0.012	0.792 ± 0.004	189.7 ± 4.3	186.1 ± 5.3	21.2 ± 2.6
1	0.005	0.724 ± 0.012	0.795 ± 0.004	189.2 ± 4.5	185.1 ± 4.7	21.1 ± 2.7
2	10^{-11}	0.728 ± 0.009	0.790 ± 0.003	196.8 ± 9.8	183.6 ± 10.6	19.1 ± 2.9
filament NF3						
0.5	10^{-11}	0.719 ± 0.010	0.787 ± 0.003	178.7 ± 1.4	189.7 ± 1.6	24.2 ± 1.4
0.5	10^{-4}	0.720 ± 0.011	0.787 ± 0.003	178.6 ± 1.6	189.3 ± 1.8	23.7 ± 1.5
0.5	0.001	0.721 ± 0.012	0.787 ± 0.003	179.6 ± 1.8	189.1 ± 2.1	24.1 ± 1.9
0.5	0.003	0.724 ± 0.012	0.787 ± 0.003	181.1 ± 1.8	188.4 ± 2.2	24.4 ± 1.7
0.5	0.005	0.724 ± 0.011	0.787 ± 0.003	180.8 ± 1.0	190.9 ± 1.7	27.0 ± 2.0
1	10^{-4}	0.723 ± 0.009	0.789 ± 0.002	179.5 ± 3.8	190.2 ± 3.4	22.7 ± 1.9
1	0.001	0.726 ± 0.014	0.786 ± 0.004	180.1 ± 3.9	191.1 ± 4.3	24.4 ± 2.4
1	0.003	0.726 ± 0.012	0.789 ± 0.004	180.6 ± 3.3	193.2 ± 3.2	25.1 ± 2.2
1	0.005	0.724 ± 0.011	0.791 ± 0.004	180.5 ± 2.6	193.9 ± 2.9	25.4 ± 2.5
filament NF4						
[0.5	10^{-4}	0.373 ± 0.046	0.878 ± 0.012	297.0 ± 16.7	79.2 ± 17.9	3.6 ± 1.1]
[1	10^{-4}	0.395 ± 0.063	0.871 ± 0.017	296.7 ± 16.9	94.9 ± 17.6	5.9 ± 1.4]
filament NF5						
0.5	0.003	0.718 ± 0.010	0.790 ± 0.002	182.3 ± 0.3	188.8 ± 1.5	24.1 ± 1.4
0.5	0.005	0.721 ± 0.004	0.791 ± 0.002	182.4 ± 0.3	190.1 ± 0.7	25.2 ± 1.0
filament NF6						
[0.5	10^{-11}	0.723 ± 0.016	0.793 ± 0.004	190.6 ± 13.2	175.7 ± 13.6	12.7 ± 2.5]
[0.5	0.003	0.703 ± 0.025	0.800 ± 0.006	211.9 ± 19.7	156.9 ± 20.8	10.3 ± 4.9]

Table 4

– continuation.

t_{ev} [kyr]	β [1]	q [au]	e	ω [deg]	Ω [deg]	i [deg]
filament SF1						
[0.5	10^{-4}	0.699 ± 0.028	0.800 ± 0.006	344.3 ± 22.5	25.8 ± 24.3	7.7 ± 2.7]
[0.5	0.005	0.639 ± 0.070	0.817 ± 0.014	309.6 ± 19.9	60.9 ± 18.2	4.3 ± 0.9]
[1	10^{-11}	0.644 ± 0.057	0.812 ± 0.013	315.8 ± 25.7	69.2 ± 24.1	6.4 ± 3.3]
[1	0.001	0.648 ± 0.052	0.815 ± 0.011	318.9 ± 28.2	59.3 ± 26.3	5.1 ± 1.7]
[1	0.003	0.630 ± 0.037	0.819 ± 0.008	321.3 ± 27.8	54.5 ± 29.7	5.6 ± 2.2]
[2	10^{-11}	0.642 ± 0.054	0.814 ± 0.012	327.1 ± 22.3	50.8 ± 23.7	6.6 ± 3.3]
[2	10^{-4}	0.644 ± 0.053	0.812 ± 0.012	318.0 ± 19.5	66.6 ± 20.2	7.4 ± 3.3]
filament SF2						
1	0.003	0.720 ± 0.013	0.788 ± 0.004	344.3 ± 3.7	30.7 ± 6.2	25.0 ± 3.0
[2	10^{-11}	0.721 ± 0.015	0.791 ± 0.003	343.8 ± 13.1	37.0 ± 16.6	18.7 ± 3.1]
[2	10^{-4}	0.714 ± 0.015	0.793 ± 0.004	343.5 ± 10.2	33.3 ± 12.9	19.0 ± 3.0]
2	0.003	0.720 ± 0.011	0.790 ± 0.004	341.6 ± 5.3	31.8 ± 4.6	20.6 ± 3.1
filament SF3						
1	0.001	0.715 ± 0.015	0.769 ± 0.008	352.9 ± 2.3	42.7 ± 2.2	38.4 ± 2.4
2	10^{-11}	0.724 ± 0.013	0.770 ± 0.011	358.9 ± 7.5	30.4 ± 11.2	36.3 ± 6.2
2	10^{-4}	0.720 ± 0.012	0.774 ± 0.006	360.0 ± 3.2	6.2 ± 6.6	34.6 ± 4.0
2	0.003	0.723 ± 0.011	0.762 ± 0.006	356.0 ± 4.5	37.0 ± 4.6	40.0 ± 2.1
2	0.005	0.725 ± 0.013	0.762 ± 0.007	353.8 ± 5.4	38.2 ± 4.4	38.8 ± 2.1

Table 5

The mean planet-centric parameters of the showers associated with the comet 21P/Giacobini-Zinner, which are predicted to be seen on Mars. The same denotation as in Table 1 is used.

t_{ev} [kyr]	β [1]	λ_{\odot} [deg]	$\lambda_{min}-\lambda_{max}$ [deg]	α [deg]	δ [deg]	V_{pc} km s ⁻¹	γ [deg]	n
filament NF1								
0.5	10 ⁻¹¹	196.1 ± 2.2	186.6–198.4	261.9 ± 1.1	65.0 ± 3.0	23.1 ± 1.3	86.	278
0.5	10 ⁻⁴	196.3 ± 2.2	189.6–198.4	261.8 ± 1.1	65.1 ± 2.9	23.2 ± 1.3	86.	284
0.5	0.001	196.1 ± 2.3	189.9–198.4	261.9 ± 1.3	64.7 ± 3.1	23.0 ± 1.4	86.	255
0.5	0.003	196.3 ± 2.4	190.8–198.3	261.9 ± 1.2	64.0 ± 3.0	22.8 ± 1.4	86.	112
0.5	0.005	186.5 ± 1.7	183.5–189.1	270.5 ± 1.9	50.7 ± 2.1	17.3 ± 0.7	89.	23
1	10 ⁻¹¹	197.6 ± 2.9	191.5–203.0	262.0 ± 2.4	64.6 ± 3.9	23.0 ± 1.8	86.	85
1	10 ⁻⁴	197.8 ± 3.2	189.4–203.9	261.7 ± 2.7	64.8 ± 4.3	23.2 ± 2.0	86.	70
1	0.001	198.2 ± 3.7	188.0–204.7	261.6 ± 3.5	65.0 ± 4.5	23.2 ± 2.1	86.	61
1	0.003	199.3 ± 3.5	191.9–206.1	261.1 ± 4.1	65.7 ± 5.4	23.7 ± 2.4	86.	31
1	0.005	193.3 ± 7.7	179.4–204.9	267.2 ± 10.6	54.0 ± 11.0	19.6 ± 4.1	86.	74
2	10 ⁻¹¹	213.4 ± 4.7	201.2–224.9	261.9 ± 6.1	64.8 ± 4.3	23.4 ± 2.0	86.	66
2	10 ⁻⁴	210.7 ± 6.7	196.9–225.4	261.8 ± 5.0	63.4 ± 3.6	22.8 ± 1.9	85.	56
2	0.001	211.4 ± 6.3	196.8–229.2	261.7 ± 4.7	63.9 ± 4.5	23.0 ± 2.1	86.	43
2	0.003	209.6 ± 6.8	190.8–223.5	264.3 ± 10.4	68.2 ± 3.3	24.5 ± 1.2	89.	52
2	0.005	210.4 ± 5.7	196.0–221.3	263.7 ± 7.1	66.8 ± 5.0	24.0 ± 1.9	88.	53
filament NF2								
0.5	10 ⁻¹¹	195.3 ± 7.3	185.4–203.1	282.7 ± 3.4	67.8 ± 1.7	23.3 ± 0.8	95.	5
1	10 ⁻¹¹	204.8 ± 1.9	195.7–208.1	280.4 ± 6.4	69.0 ± 3.5	23.4 ± 1.9	95.	46
1	10 ⁻⁴	204.5 ± 2.6	194.6–208.9	280.3 ± 5.3	69.7 ± 2.8	23.8 ± 1.6	95.	47
1	0.001	204.3 ± 2.7	193.2–210.2	277.6 ± 5.3	71.0 ± 1.5	24.5 ± 1.0	94.	30
1	0.003	197.4 ± 8.5	185.1–209.6	278.3 ± 8.0	61.2 ± 8.9	20.9 ± 3.4	92.	15
2	10 ⁻¹¹	209.0 ± 3.9	201.2–215.3	270.2 ± 6.7	69.0 ± 3.2	24.1 ± 1.0	91.	19
2	10 ⁻⁴	206.9 ± 7.4	185.1–217.0	269.5 ± 10.2	68.1 ± 3.3	23.8 ± 1.5	91.	19
2	0.001	190.3 ± 14.2	171.5–210.1	280.3 ± 7.9	67.1 ± 3.9	23.2 ± 1.7	94.	6
filament NF3								
[0.5	10 ⁻¹¹	170.3 ± 2.8	165.6–173.5	264.9 ± 25.1	17.3 ± 5.9	11.5 ± 0.7	92.	8]
1	10 ⁻¹¹	180.1 ± 5.3	171.5–187.8	274.8 ± 3.3	38.2 ± 9.8	14.1 ± 2.4	94.	25
1	10 ⁻⁴	180.9 ± 5.9	168.5–189.1	274.2 ± 5.0	41.2 ± 9.1	14.5 ± 2.4	93.	19
1	0.001	184.8 ± 4.5	175.8–190.9	274.0 ± 2.8	45.3 ± 7.4	15.9 ± 1.7	91.	26
1	0.003	181.0 ± 5.1	170.6–186.0	274.8 ± 6.2	41.1 ± 5.8	13.4 ± 3.0	93.	12

Table 5
– continuation.

t_{ev} [kyr]	β [1]	λ_{\odot} [deg]	$\lambda_{min}-\lambda_{max}$ [deg]	α [deg]	δ [deg]	V_{pc} km s ⁻¹	γ [deg]	n
filament NF4								
[0.5	10^{-11}	98.2 ± 14.9	77.4–117.2	286.1 ± 12.4	-16.9 ± 3.7	28.7 ± 2.0	171.	12]
[0.5	10^{-4}	82.1 ± 6.7	72.6– 91.7	272.2 ± 4.9	-20.9 ± 1.2	30.2 ± 1.5	170.	10]
[0.5	0.001	87.9 ± 6.9	78.4– 99.9	276.8 ± 5.0	-21.0 ± 1.2	29.3 ± 1.6	171.	12]
[0.5	0.003	70.8 ± 11.4	61.0– 90.5	264.3 ± 9.7	-21.9 ± 0.6	32.6 ± 2.4	166.	7]
[0.5	0.005	83.8 ± 20.5	62.0–115.8	269.4 ± 14.7	-19.6 ± 2.9	28.0 ± 3.6	173.	5]
[1	10^{-11}	107.6 ± 45.7	77.7–341.2	289.3 ± 9.9	-17.6 ± 3.2	29.7 ± 2.1	175.	47]
[1	10^{-4}	100.9 ± 13.6	75.0–135.7	290.4 ± 10.3	-16.8 ± 3.5	29.4 ± 2.5	170.	37]
1	0.001	104.2 ± 7.3	90.9–117.8	293.2 ± 5.5	-16.0 ± 2.6	29.0 ± 1.6	170.	29
2	10^{-11}	115.4 ± 8.7	100.8–126.4	305.2 ± 5.8	-12.5 ± 3.6	29.4 ± 1.8	169.	7
[2	10^{-4}	106.8 ± 13.0	88.6–121.0	297.2 ± 9.2	-16.4 ± 2.6	29.6 ± 2.5	170.	7]
[2	0.001	110.2 ± 18.8	77.3–143.2	292.7 ± 13.3	-14.5 ± 6.0	26.2 ± 4.0	173.	20]
[2	0.003	112.2 ± 15.5	92.6–136.2	296.5 ± 8.0	-12.8 ± 5.6	26.9 ± 3.9	171.	9]
2	0.005	104.2 ± 8.2	92.0–114.1	296.8 ± 5.6	-16.4 ± 2.8	30.6 ± 1.6	168.	7
filament NF5								
1	10^{-11}	169.0 ± 8.0	156.6–178.5	236.8 ± 17.0	20.0 ± 8.4	12.0 ± 0.7	67.	5
[1	0.001	172.2 ± 4.8	163.5–181.4	244.8 ± 27.8	21.1 ± 12.0	12.0 ± 2.9	72.	10]
filament NF6								
4	10^{-4}	346.0 ± 6.2	338.2–355.1	272.7 ± 8.4	67.1 ± 5.6	20.9 ± 2.3	89.	6
filament NF7								
4	10^{-4}	226.5 ± 6.9	219.3–237.2	297.3 ± 22.8	55.8 ± 4.2	16.8 ± 2.8	95.	8
filament NF8								
[2	10^{-11}	215.5 ± 7.3	193.3–230.6	324.8 ± 29.7	43.7 ± 7.4	14.8 ± 1.4	115.	52]
[2	10^{-4}	213.7 ± 9.1	192.5–232.0	308.5 ± 33.6	46.9 ± 8.5	15.8 ± 1.7	104.	47]
[2	0.001	216.6 ± 3.7	205.6–224.6	328.4 ± 30.4	44.1 ± 7.8	15.3 ± 1.2	117.	36]
[2	0.005	216.7 ± 5.6	197.7–225.7	327.8 ± 29.7	44.1 ± 8.2	15.2 ± 1.4	116.	38]
filament NF9								
[1	0.003	328.4 ± 14.6	310.9–351.0	319.8 ± 11.1	-13.8 ± 3.7	30.0 ± 2.7	11.	9]
[2	10^{-11}	319.0 ± 9.5	307.6–333.9	313.2 ± 7.2	-14.0 ± 3.5	28.3 ± 2.2	8.	5]
filament NF10								
2	10^{-11}	220.1 ± 8.3	204.5–230.2	276.3 ± 4.6	-10.0 ± 3.3	9.7 ± 1.7	57.	15
2	10^{-4}	218.8 ± 8.1	200.0–229.7	275.9 ± 4.0	-10.6 ± 2.4	9.5 ± 1.6	58.	15
2	0.001	220.2 ± 8.4	203.1–230.2	277.4 ± 4.4	-10.9 ± 2.3	9.6 ± 1.9	58.	19
2	0.003	221.5 ± 9.6	204.9–229.6	276.8 ± 3.2	-10.0 ± 4.4	9.9 ± 2.0	56.	12
2	0.005	208.8 ± 3.3	204.5–212.0	283.4 ± 3.4	-12.5 ± 3.8	7.6 ± 0.7	75.	6
filament NF11								
2	10^{-4}	214.2 ± 4.2	206.6–221.5	273.6 ± 2.6	8.3 ± 4.5	6.8 ± 0.5	65.	11
2	0.003	217.7 ± 4.5	212.9–227.4	274.2 ± 3.1	7.6 ± 5.8	7.2 ± 0.5	62.	9

Table 5
– continuation.

t_{ev} [kyr]	β [1]	λ_{\odot} [deg]	$\lambda_{min}-\lambda_{max}$ [deg]	α [deg]	δ [deg]	V_{pc} km s^{-1}	γ [deg]	n
filament SF1								
0.5	10^{-4}	230.5 ± 20.3	204.2–257.2	257.3 ± 9.5	-29.5 ± 1.4	15.7 ± 2.7	29.	8
[0.5	0.003	248.9 ± 8.9	239.1–264.6	264.9 ± 5.4	-28.5 ± 2.1	18.5 ± 1.9	17.	6]
[1	10^{-11}	247.6 ± 27.9	195.6–280.1	274.3 ± 13.8	-28.1 ± 1.8	17.5 ± 5.1	27.	18]
[1	0.003	243.5 ± 16.7	215.9–260.1	271.7 ± 4.8	-30.3 ± 2.5	16.4 ± 3.6	29.	10]
[1	0.005	245.2 ± 29.2	159.8–262.7	272.0 ± 13.3	-29.5 ± 3.2	18.7 ± 2.3	27.	11]
2	10^{-11}	233.8 ± 10.8	214.5–244.9	271.1 ± 2.5	-32.5 ± 2.9	13.8 ± 1.9	38.	8
filament SF2								
[0.5	10^{-11}	197.8 ± 11.0	187.8–210.0	88.5 ± 15.0	-68.3 ± 9.0	22.8 ± 4.1	90.	5]
[2	10^{-4}	203.5 ± 10.8	184.6–221.3	81.8 ± 25.5	-68.1 ± 6.0	22.1 ± 3.8	92.	7]
[2	0.003	198.7 ± 10.4	186.2–217.5	83.0 ± 18.6	-70.6 ± 8.5	21.5 ± 3.5	91.	9]
2	0.005	168.2 ± 3.7	163.1–173.5	92.7 ± 4.0	-63.3 ± 1.2	24.7 ± 0.7	88.	8
4	10^{-4}	175.3 ± 6.1	169.5–183.3	79.7 ± 7.3	-68.3 ± 4.0	22.4 ± 2.0	94.	5
filament SF3								
0.5	10^{-4}	300.5 ± 3.5	294.7–303.3	294.5 ± 2.5	-25.3 ± 0.5	29.2 ± 0.8	9.	5
[0.5	0.001	296.4 ± 17.3	272.2–321.2	292.3 ± 12.7	-25.7 ± 3.1	28.2 ± 4.0	7.	11]
1	10^{-11}	318.9 ± 6.8	307.1–331.5	315.0 ± 4.4	-23.9 ± 2.0	28.9 ± 1.6	11.	23
1	10^{-4}	317.2 ± 5.4	304.1–327.1	314.4 ± 3.1	-24.5 ± 1.8	28.3 ± 1.2	10.	23
1	0.001	317.7 ± 4.8	309.2–325.2	314.6 ± 3.1	-24.1 ± 1.7	28.4 ± 1.1	10.	15
[2	10^{-4}	295.9 ± 22.1	264.8–333.1	304.1 ± 17.7	-29.3 ± 6.8	23.2 ± 3.5	10.	18]
[2	0.001	280.0 ± 10.7	266.6–298.5	294.4 ± 9.5	-30.6 ± 5.7	20.2 ± 1.3	14.	14]
filament SF4								
[0.5	10^{-4}	152.0 ± 6.5	144.6–158.8	307.4 ± 6.7	-25.7 ± 3.6	15.1 ± 1.6	151.	5]
[0.5	0.001	150.2 ± 32.8	120.7–190.2	278.9 ± 21.0	-25.9 ± 2.4	14.9 ± 5.6	128.	7]
[2	10^{-11}	160.1 ± 26.2	126.2–185.7	320.6 ± 13.7	-24.0 ± 5.9	16.7 ± 4.1	154.	6]
2	0.001	166.5 ± 7.4	156.0–173.9	311.5 ± 3.0	-32.7 ± 3.6	12.8 ± 1.4	137.	10
[2	0.003	154.7 ± 18.6	130.2–174.3	304.7 ± 9.5	-29.6 ± 4.2	14.1 ± 2.5	144.	9]
2	0.005	159.5 ± 7.1	147.5–173.8	312.1 ± 4.0	-34.5 ± 4.1	14.2 ± 1.5	142.	16
4	10^{-11}	150.3 ± 21.1	123.8–175.3	311.0 ± 11.1	-38.1 ± 6.2	16.1 ± 3.3	147.	6
[4	0.003	131.6 ± 21.0	107.7–162.0	289.1 ± 23.5	-32.9 ± 4.5	16.4 ± 2.9	153.	9]
filament SF5								
[0.5	10^{-4}	172.9 ± 4.8	168.4–181.0	260.7 ± 49.5	-62.9 ± 6.1	11.8 ± 1.0	91.	5]
0.5	0.001	177.9 ± 4.8	172.8–184.0	308.3 ± 60.8	-70.7 ± 11.5	11.7 ± 3.1	103.	5
2	0.001	180.3 ± 2.7	177.0–183.5	218.3 ± 8.9	-74.3 ± 7.3	13.0 ± 0.5	78.	5
[4	10^{-11}	148.1 ± 8.6	139.2–161.1	141.4 ± 39.4	-69.6 ± 5.5	16.7 ± 3.9	82.	7]
4	0.001	180.6 ± 5.1	173.0–186.6	194.5 ± 74.9	-80.9 ± 8.4	15.8 ± 3.5	81.	5

Table 6

The mean orbital elements of the showers associated with the comet 21P, which are predicted to be detected on Mars. Quantities t_{ev} and β are the same as in Table 1.

t_{ev} [kyr]	β [1]	q [au]	e	ω [deg]	Ω [deg]	i [deg]
filament NF1						
0.5	10^{-11}	1.401 ± 0.014	0.615 ± 0.013	169.9 ± 3.8	199.2 ± 1.2	37.7 ± 2.6
0.5	10^{-4}	1.402 ± 0.015	0.614 ± 0.012	170.0 ± 3.7	199.4 ± 1.1	37.9 ± 2.5
0.5	0.001	1.399 ± 0.014	0.617 ± 0.013	169.4 ± 3.8	199.3 ± 1.1	37.5 ± 2.8
0.5	0.003	1.394 ± 0.012	0.621 ± 0.012	168.5 ± 3.7	199.8 ± 1.0	37.0 ± 2.7
0.5	0.005	1.373 ± 0.008	0.667 ± 0.004	161.6 ± 1.0	194.8 ± 1.4	26.1 ± 1.5
1	10^{-11}	1.405 ± 0.016	0.614 ± 0.017	169.6 ± 4.6	200.9 ± 1.6	37.5 ± 3.6
1	10^{-4}	1.402 ± 0.017	0.614 ± 0.017	169.7 ± 4.9	201.0 ± 1.9	37.8 ± 3.9
1	0.001	1.406 ± 0.017	0.613 ± 0.018	169.8 ± 5.8	201.4 ± 2.2	38.0 ± 4.1
1	0.003	1.406 ± 0.018	0.615 ± 0.024	170.3 ± 7.8	202.4 ± 1.9	38.8 ± 4.8
1	0.005	1.383 ± 0.021	0.658 ± 0.032	161.2 ± 3.3	201.2 ± 4.7	30.3 ± 8.6
2	10^{-11}	1.424 ± 0.018	0.606 ± 0.017	167.5 ± 11.0	217.4 ± 7.0	38.4 ± 3.7
2	10^{-4}	1.422 ± 0.019	0.612 ± 0.019	165.0 ± 7.0	215.4 ± 7.8	37.2 ± 3.7
2	0.001	1.416 ± 0.021	0.611 ± 0.019	165.6 ± 9.3	216.0 ± 7.2	37.7 ± 4.1
2	0.003	1.417 ± 0.019	0.599 ± 0.013	178.4 ± 13.9	210.5 ± 7.9	40.6 ± 2.4
2	0.005	1.417 ± 0.017	0.602 ± 0.018	173.4 ± 13.7	212.9 ± 8.0	39.6 ± 3.6
filament NF2						
0.5	10^{-11}	1.381 ± 0.017	0.616 ± 0.010	197.4 ± 4.0	192.0 ± 7.5	38.3 ± 1.5
1	10^{-11}	1.395 ± 0.022	0.606 ± 0.017	197.7 ± 6.6	201.1 ± 1.9	38.6 ± 3.7
1	10^{-4}	1.395 ± 0.021	0.605 ± 0.014	197.0 ± 5.4	201.1 ± 2.4	39.3 ± 3.0
1	0.001	1.407 ± 0.014	0.598 ± 0.009	194.7 ± 4.7	201.7 ± 2.8	40.7 ± 1.9
1	0.003	1.373 ± 0.030	0.642 ± 0.031	188.4 ± 22.0	196.4 ± 8.8	33.4 ± 6.7
2	10^{-11}	1.425 ± 0.019	0.600 ± 0.011	185.1 ± 10.3	208.6 ± 3.9	39.8 ± 2.2
2	10^{-4}	1.416 ± 0.024	0.604 ± 0.015	183.7 ± 13.7	206.6 ± 7.1	39.3 ± 2.9
2	0.001	1.380 ± 0.035	0.615 ± 0.019	196.4 ± 9.6	187.0 ± 13.7	38.1 ± 3.2
filament NF3						
[0.5	10^{-11}	1.370 ± 0.019	0.689 ± 0.003	179.1 ± 16.8	172.2 ± 16.1	$10.7 \pm 2.1]$
1	10^{-11}	1.374 ± 0.013	0.678 ± 0.011	166.4 ± 6.2	188.3 ± 6.9	19.0 ± 4.9
1	10^{-4}	1.372 ± 0.016	0.675 ± 0.011	165.5 ± 6.3	189.2 ± 8.0	20.2 ± 4.6
1	0.001	1.376 ± 0.011	0.669 ± 0.011	163.6 ± 3.8	193.3 ± 4.7	22.9 ± 3.9
1	0.003	1.375 ± 0.014	0.684 ± 0.008	166.0 ± 8.2	189.5 ± 8.6	18.6 ± 3.9

Table 6
– continuation.

t_{ev} [kyr]	β [1]	q [au]	e	ω [deg]	Ω [deg]	i [deg]
filament NF4						
[0.5	10^{-11}	0.415 ± 0.070	0.866 ± 0.018	307.1 ± 19.1	77.4 ± 21.9	6.2 ± 2.8
[0.5	10^{-4}	0.362 ± 0.051	0.881 ± 0.014	301.2 ± 18.5	73.0 ± 19.4	3.2 ± 1.3
[0.5	0.001	0.389 ± 0.055	0.873 ± 0.014	312.8 ± 21.6	64.1 ± 22.5	3.0 ± 1.0
[0.5	0.003	0.283 ± 0.073	0.903 ± 0.021	326.0 ± 22.1	46.3 ± 18.1	2.1 ± 1.0
[0.5	0.005	0.437 ± 0.129	0.861 ± 0.029	297.0 ± 26.3	70.2 ± 27.9	3.4 ± 1.6
[1	10^{-11}	0.378 ± 0.072	0.876 ± 0.019	321.9 ± 26.5	67.0 ± 27.9	5.8 ± 3.0
[1	10^{-4}	0.389 ± 0.087	0.873 ± 0.023	310.6 ± 17.9	79.7 ± 18.3	6.1 ± 2.5
1	0.001	0.404 ± 0.055	0.868 ± 0.015	315.3 ± 9.0	76.6 ± 11.1	7.1 ± 2.2
2	10^{-11}	0.391 ± 0.071	0.871 ± 0.019	315.5 ± 8.8	89.3 ± 9.9	8.6 ± 2.2
[2	10^{-4}	0.381 ± 0.084	0.875 ± 0.022	314.5 ± 16.7	82.6 ± 19.6	6.1 ± 3.7
[2	0.001	0.506 ± 0.148	0.845 ± 0.035	294.0 ± 28.4	91.9 ± 29.7	5.7 ± 3.0
[2	0.003	0.480 ± 0.147	0.850 ± 0.034	295.4 ± 26.4	95.5 ± 24.7	7.7 ± 3.0
2	0.005	0.339 ± 0.055	0.882 ± 0.015	319.9 ± 5.6	79.7 ± 7.6	6.6 ± 3.2
filament NF5						
1	10^{-11}	1.356 ± 0.051	0.695 ± 0.004	201.9 ± 12.1	153.7 ± 10.8	11.2 ± 3.5
[1	0.001	1.369 ± 0.038	0.697 ± 0.007	195.0 ± 18.8	161.0 ± 19.7	10.8 ± 2.6
filament NF6						
4	10^{-4}	1.616 ± 0.025	0.556 ± 0.026	156.1 ± 6.8	354.0 ± 6.6	35.0 ± 4.4
filament NF7						
4	10^{-4}	1.410 ± 0.042	0.646 ± 0.023	147.2 ± 6.7	243.2 ± 8.3	25.7 ± 5.9
filament NF8						
[2	10^{-11}	1.371 ± 0.049	0.680 ± 0.012	143.2 ± 13.8	240.8 ± 16.6	18.0 ± 4.2
[2	10^{-4}	1.381 ± 0.047	0.670 ± 0.017	149.0 ± 16.2	233.3 ± 19.5	21.1 ± 5.6
[2	0.001	1.366 ± 0.046	0.679 ± 0.014	139.8 ± 10.5	244.4 ± 11.6	18.2 ± 4.7
[2	0.003	1.390 ± 0.039	0.656 ± 0.027	151.5 ± 12.0	228.4 ± 16.6	25.8 ± 7.8
[2	0.005	1.365 ± 0.043	0.682 ± 0.016	139.8 ± 10.4	244.5 ± 12.5	18.2 ± 4.7
filament NF9						
[1	0.003	0.359 ± 0.092	0.881 ± 0.025	14.2 ± 13.3	22.8 ± 14.7	3.2 ± 1.0
[2	10^{-11}	0.420 ± 0.077	0.865 ± 0.021	30.8 ± 18.5	4.2 ± 11.8	4.5 ± 2.6
filament NF10						
2	10^{-11}	1.066 ± 0.047	0.732 ± 0.007	96.7 ± 4.0	285.4 ± 4.6	11.4 ± 1.2
2	10^{-4}	1.070 ± 0.045	0.732 ± 0.006	96.3 ± 3.6	285.3 ± 3.9	11.4 ± 1.3
2	0.001	1.067 ± 0.057	0.733 ± 0.008	95.9 ± 4.6	286.8 ± 4.5	11.2 ± 1.3
2	0.003	1.062 ± 0.062	0.735 ± 0.008	96.5 ± 5.9	286.1 ± 4.8	11.3 ± 1.2
2	0.005	1.111 ± 0.036	0.728 ± 0.004	99.7 ± 2.8	283.4 ± 2.5	9.2 ± 0.9
filament NF11						
2	10^{-4}	1.223 ± 0.013	0.709 ± 0.003	113.5 ± 3.3	270.8 ± 3.2	12.1 ± 1.5
2	0.003	1.206 ± 0.034	0.711 ± 0.006	111.8 ± 4.0	274.2 ± 5.1	12.6 ± 1.2

Table 6
– continuation.

t_{ev} [kyr]	β [1]	q [au]	e	ω [deg]	Ω [deg]	i [deg]
filament SF1						
0.5	10^{-4}	0.855 ± 0.081	0.771 ± 0.015	288.3 ± 8.6	76.6 ± 15.1	3.4 ± 0.7
[0.5	0.003	0.768 ± 0.064	0.790 ± 0.013	294.6 ± 12.7	74.5 ± 13.6	$2.9 \pm 1.4]$
[1	10^{-11}	0.786 ± 0.154	0.787 ± 0.029	299.9 ± 14.3	74.6 ± 13.6	$3.0 \pm 1.5]$
[1	0.003	0.829 ± 0.099	0.781 ± 0.019	305.8 ± 24.9	69.7 ± 23.3	$3.4 \pm 1.4]$
[1	0.005	0.764 ± 0.077	0.795 ± 0.013	309.4 ± 29.9	62.8 ± 28.3	$3.6 \pm 1.5]$
2	10^{-11}	0.919 ± 0.054	0.762 ± 0.011	289.0 ± 10.6	89.2 ± 9.9	5.3 ± 2.4
filament SF2						
[0.5	10^{-11}	1.406 ± 0.035	0.613 ± 0.036	355.7 ± 15.7	20.0 ± 11.4	$37.2 \pm 8.1]$
[2	10^{-4}	1.391 ± 0.018	0.625 ± 0.027	349.4 ± 18.8	28.4 ± 15.8	$35.9 \pm 7.3]$
[2	0.003	1.383 ± 0.033	0.628 ± 0.032	358.4 ± 21.1	19.8 ± 16.3	$34.7 \pm 7.0]$
2	0.005	1.382 ± 0.013	0.603 ± 0.004	356.4 ± 4.9	349.4 ± 3.4	41.0 ± 1.4
4	10^{-4}	1.367 ± 0.021	0.622 ± 0.014	13.2 ± 8.0	352.5 ± 5.2	36.5 ± 3.8
filament SF3						
0.5	10^{-4}	0.395 ± 0.029	0.872 ± 0.008	259.2 ± 6.7	114.8 ± 7.1	$4.2 \pm 0.7]$
[0.5	0.001	0.431 ± 0.138	0.864 ± 0.034	259.9 ± 16.9	114.2 ± 16.9	$4.3 \pm 1.1]$
1	10^{-11}	0.408 ± 0.055	0.867 ± 0.015	243.7 ± 7.0	149.6 ± 8.1	7.4 ± 1.3
1	10^{-4}	0.427 ± 0.045	0.862 ± 0.012	245.5 ± 5.8	148.4 ± 5.7	7.5 ± 0.8
1	0.001	0.422 ± 0.041	0.863 ± 0.011	246.7 ± 5.9	147.2 ± 7.1	7.2 ± 1.3
[2	10^{-4}	0.612 ± 0.133	0.820 ± 0.030	280.2 ± 23.0	115.1 ± 30.3	7.6 ± 2.6
[2	0.001	0.713 ± 0.048	0.799 ± 0.010	295.7 ± 21.9	96.7 ± 20.0	$5.6 \pm 2.6]$
filament SF4						
[0.5	10^{-4}	0.867 ± 0.050	0.769 ± 0.009	41.8 ± 14.3	337.4 ± 20.3	$2.7 \pm 0.6]$
[0.5	0.001	0.890 ± 0.191	0.768 ± 0.033	27.3 ± 23.6	342.3 ± 23.2	$1.9 \pm 0.5]$
[2	10^{-11}	0.812 ± 0.129	0.780 ± 0.023	40.8 ± 29.5	-6.6 ± 32.3	$4.7 \pm 2.5]$
2	0.001	0.987 ± 0.045	0.745 ± 0.007	82.8 ± 10.5	298.3 ± 8.7	11.2 ± 1.4
[2	0.003	0.922 ± 0.089	0.758 ± 0.016	66.8 ± 24.4	309.4 ± 18.7	$7.1 \pm 4.4]$
2	0.005	0.945 ± 0.040	0.755 ± 0.008	80.0 ± 7.8	300.4 ± 7.7	10.8 ± 1.7
4	10^{-11}	0.882 ± 0.123	0.762 ± 0.023	66.3 ± 9.8	312.9 ± 11.5	9.4 ± 3.3
[4	0.003	0.855 ± 0.089	0.765 ± 0.018	74.6 ± 8.1	288.1 ± 15.1	$6.5 \pm 3.4]$
filament SF5						
[0.5	10^{-4}	1.348 ± 0.060	0.691 ± 0.005	3.5 ± 19.9	353.0 ± 16.3	$12.3 \pm 3.1]$
0.5	0.001	1.384 ± 0.019	0.684 ± 0.007	342.8 ± 7.9	10.9 ± 8.3	14.1 ± 4.5
2	0.001	1.205 ± 0.030	0.704 ± 0.007	39.4 ± 5.2	340.2 ± 5.9	16.9 ± 1.8
[4	10^{-11}	1.355 ± 0.049	0.650 ± 0.028	10.6 ± 16.4	323.2 ± 14.8	$24.8 \pm 8.3]$
4	0.001	1.285 ± 0.049	0.676 ± 0.026	29.4 ± 5.6	348.3 ± 8.2	23.1 ± 7.2